Electromagnetic radiation detectors based on Josephson junctions: Effective Hamiltonian

D. V. Anghel,[1] K. Kulikov,[2] Y. M. Galperin,[3] and L. S. Kuzmin[4]
[1]*Horia Hulubei National Institute for R&D in Physics and Nuclear Engineering, Măgurele, Romania*
[2]*Joint Institute for Nuclear Research, Dubna, Moscow region, 141980 Russia*
[3]*Department of Physics, University of Oslo, PO Box 1048 Blindern, 0316 Oslo, Norway*
and A. F. Ioffe Physico-Technical Institute of Russian Academy of Sciences, 194021 St. Petersburg, Russia
[4]*Chalmers University of Technology, Gothenburg 41296, Sweden*
and Nizhny Novgorod State Technical University, Nizhny Novgorod 603951, Russia

(Received 7 July 2019; revised manuscript received 18 November 2019; published 17 January 2020)

We theoretically analyze two setups of low-energy single-photon counters based on Josephson junctions (JJs). For this, we propose two simple and general models based on the macroscopic quantum tunneling formalism (MQT). The first setup is similar to the photon counter based on the "cold-electron bolometer" (CEB), where the JJ replaces the CEB in the center of the superconducting antenna. In the second setup, the JJ is capacitively coupled to the antenna. We derive the Hamiltonians for the two setups, and we write the Schrödinger equations, taking into account both the antenna and the JJ. The quantum particles of the MQT models move in two-dimensional potential landscapes, which are parabolic along one direction and may have the form of a washboard potential along another direction. Such a potential landscape has a series of local minima, separated by saddle points. If the particle is prepared in the initial state in the metastable "ground state" of a local minimum, then the photon absorption causes it to jump into an excited state. If the excitation energy is bigger than the potential barrier seen by the quantum particle (the difference between the ground state and the saddle point), the photon is detected. The models are simple and allow us to do mostly analytical calculations. We show that the two setups are equivalent from the MQT point of view since one Hamiltonian can be transformed into the other by changes in variables. For typical values of the JJ and antenna parameters, the setups may work as counters of photons of wavelengths up to at least 1 cm. Dark count rates due to the phase particle tunneling directly from the ground state into the running state have also been evaluated.

DOI: 10.1103/PhysRevB.101.024511

I. INTRODUCTION

Photon counters are required for a variety of applications, such as radiation-matter interaction, quantum optics, astrophysics, atomic physics, and quantum information processing [1–9]. Furthermore, the race to detect centimeter-long-wavelength photons was intensified by the proposal that axions—the elusive particles of the standard model that might participate in the formation of dark matter [10–13]—could be detected after they decay into such photons when they pass through a region of high magnetic field [14,15]. Eventually, the most promising technologies that may be employed for detecting photons of centimeter-long wavelength are based on superconducting devices [1–9,16–31]. However, to detect axions these detectors have to be coupled to an antenna and should monitor the environment for rare events—eventually, one in a few hours. For example, the cold-electron bolometer (CEB) [21–23] was proposed as a counter [24] for photons of wavelengths up to 1 cm [32]. The CEB is capacitively coupled to an antenna that absorbs the photon. The energy of the photon is dissipated into the normal-metal island of the CEB, causing a rise in the electron temperature in the normal metal, which may be detected by the normal-metal-insulator-superconductor (NIS) tunnel junctions [1,33,34].

Another method to detect microwave photons produced by axions is using Josephson junctions (JJs) [35–37] as photon counters [25–29]. At a bias current lower than the critical current, the JJ may be in the superconducting (nondissipative) regime, where its dynamics is described along the macroscopic quantum tunneling (MQT) formalism, as a quantum particle in a washboard potential. Coupled to an antenna, which can absorb the photon, the quantum particle representing the JJ may be excited and escape over the barrier created by the washboard potential or may tunnel through it. Such a process would put the system into the running state; the JJ becomes dissipative, and the photon is detected.

We shall present two setups for the construction of the JJ detector. The first setup is based on the design of the photon counter with a CEB, such as the one proposed in [24,32]. In this setup, the CEB is replaced by a current-biased JJ, which is placed in the center of a superconducting antenna and is electrically connected in series with it. In the second setup, the antenna is capacitively connected to the JJ, as shown, for example, in Ref. [29].

In this paper, we present the MQT description of the whole system in both setups; that is, we include in the description the JJ, as well as the antenna. The photon absorption is seen as a single excitation of the system, which may (or may not) drive the quantum particle over the potential barrier. To simplify the description so that we can do mostly analytical calculations and capture the essential physical phenomena, we do not describe the environment of the JJ in full detail (i.e.,

 ©2020 American Physical Society

as a transmission line coupled to the JJ [29]), but we shall model it as a simple *LC* circuit coupled to the JJ. We observe that the MQT quantum particle moves in a two-dimensional (2D) potential landscape. Depending on the parameters of the system, the potential energy may look like a 2D washboard potential (which is concave in a direction which is not along the washboard potential), with an infinite number of local minima and saddle points between them. The absorption of a photon excites the MQT particle, which may be in the metastable ground state of one of the local minima. If the excitation energy (i.e., the photon's energy) exceeds the difference between the ground-state energy (in which the MQT particle stays) and the closest saddle point energy, then the system gets into the running state, the JJ becomes dissipative, and a voltage pulse is detected in the circuit, which counts the photon. Certainly, the system may get into the running state after the absorption of the photon by tunneling through the potential barrier. In this paper, we focus on derivation of the effective Hamiltonian of the device. Its quantum dynamics, including an interplay between activation and tunneling, as well as thermalization after an absorption event, will be considered elsewhere. Such an analysis will allow estimating the "dead time" of the detector after counting of a photon. We shall see that the two experimental setups are equivalent, as one can transform the Hamiltonian of one system into the Hamiltonian of the other by a change in variables.

This paper is organized as follows. In the next section we present the electric circuit diagrams for the two setups and the corresponding quantum descriptions. By algebraic manipulations, we bring the two Hamiltonian operators to the same form and investigate the properties of the potential energy landscape. We find analytically the positions of the minima, the saddle points, and the difference in energy between consecutive minima and saddle points. To find the (metastable) ground-state energy, we approximate the Hamiltonian around a local minimum with a harmonic potential and calculate the energy of the ground state to finally calculate the energy required to bring the system into the running state and detect the photon. We investigate whether the system can be realized using concrete physical parameters. The last section is reserved for conclusions.

II. METHODS

The experimental setups that we are going to describe are similar to the ones presented in Refs. [24] (*first setup*) and [29] (*second setup*). In the first setup, the CEB is replaced with the JJ, which is connected in series with the superconducting antenna. In the second setup, the JJ is capacitively connected with the antenna. In both cases, the antenna is described as a simple *LC* circuit of inductance L_A and capacitance C_A. Similarly, the JJ in both cases has the parameters E_c (charge energy), capacitance C_J, critical current I_c, and instantaneous current I_J. The two equivalent circuits are presented in Figs. 1 and 2.

A. First setup

The equivalent electrical circuit of the first setup [24] is presented in Fig. 1. The JJ is placed in series with the superconducting antenna and is current biased. The total current through the circuit is the external current I and the total voltage is V_T. If the current through the junction I_J is smaller than the critical current I_c, then the JJ is in the superconducting state, and we can write $I_J = I_c \sin\phi_J$, where ϕ_J is the phase drop on the junction. Similarly, the current through L_A is I_A; the charges on the capacitors are $Q_A = V_T C_A$ and $Q_J = V_J C_J$. Then, the energy of the JJ is [36]

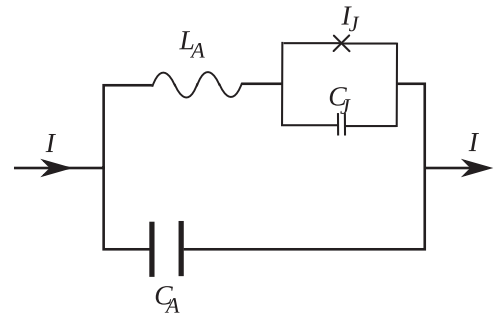

FIG. 1. The equivalent circuit of the detector in the *first setup*. The current through the JJ is I_J, and the capacitance is C_J. The superconducting antenna of impedance L_A and capacitance C_A is connected in series with the JJ.

$$E_J = \frac{C_J V_J^2}{2} + E_c(1-\cos\phi_J) \equiv \frac{Q_J^2}{2C_J} + E_c(1-\cos\phi_J,) \tag{1a}$$

whereas the energy in the antenna is

$$E_A = \frac{C_A V_T^2}{2} + \frac{L_A I_A^2}{2} \equiv \frac{Q_A^2}{2C_A} + \frac{L_A I_A^2}{2}. \tag{1b}$$

The total energy of the system is

$$E_T^{(1)} = E_J + E_A. \tag{1c}$$

Since $E_T^{(1)}$ is not conserved because of the power supplied from the external circuit, $P_{\text{ext}} \equiv IV_T$, we introduce the overall phase

$$\phi_T(t) = \frac{2e}{\hbar}\int_{-\infty}^{t} dt'\, V_T(t') \;\Leftrightarrow\; \dot{\phi}_T = \frac{2e}{\hbar} V_T(t) \tag{2}$$

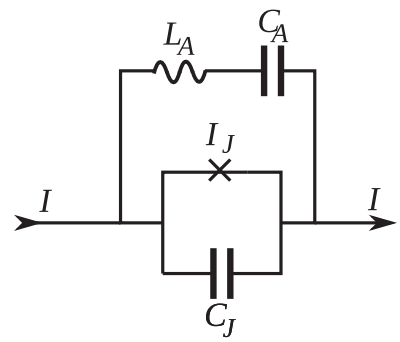

FIG. 2. The equivalent circuit of the detector in the *second setup*. The current through the JJ is I_J, and the capacitance is C_J. The superconducting antenna of impedance L_A and capacitance C_A is capacitively connected with the JJ.

and write the Hamiltonian

$$H^{(1)} = E_T^{(1)} - \frac{\hbar}{2e} I\phi_T, \tag{3}$$

which is conserved and may be used in the MQT procedure [37].

If we denote by V_A the voltage on L_A and since V_T is the voltage on C_A, then we have $V_T = V_J + V_A$, which implies

$$\phi_T = \phi_J + \phi_A, \tag{4}$$

where

$$\phi_A = \frac{2e}{\hbar}\int_{-\infty}^{t} dt'\, V_A(t'). \tag{5}$$

Putting together Eqs. (1)–(5), we obtain the total Hamiltonian of the system in terms of ϕ_T and ϕ_J,

$$H^{(1)} = \frac{C_A}{2}\left(\frac{\hbar}{2e}\right)^2\dot{\phi}_T^2 + \frac{1}{2L_A}\left(\frac{\hbar}{2e}\right)^2\phi_T^2 - \frac{\hbar}{2e}I\phi_T + \frac{C_J}{2}\left(\frac{\hbar}{2e}\right)^2\dot{\phi}_J^2 + E_c(1-\cos\phi_J) + \frac{1}{2L_A}\left(\frac{\hbar}{2e}\right)^2\phi_J^2 - \frac{1}{L_A}\left(\frac{\hbar}{2e}\right)^2\phi_T\phi_J. \tag{6}$$

From Eq. (6) we calculate the conjugate momenta of variables ϕ_T and ϕ_J,

$$p_T = \frac{\partial H^{(1)}}{\partial\dot{\phi}_T} = C_A\left(\frac{\hbar}{2e}\right)^2\dot{\phi}_T = C_A\frac{\hbar}{2e}V_T \equiv \frac{\hbar}{2e}Q_A, \tag{7a}$$

$$p_J = \frac{\partial H^{(1)}}{\partial\dot{\phi}_J} = C_J\left(\frac{\hbar}{2e}\right)^2\dot{\phi}_J = C_J\frac{\hbar}{2e}V_J \equiv \frac{\hbar}{2e}Q_J. \tag{7b}$$

We write the quantum-mechanical Hamiltonian as

$$\hat{H}^{(1)} = -\frac{\hbar^2}{2C_A}\left(\frac{2e}{\hbar}\right)^2\frac{\partial^2}{\partial\phi_T^2} + \frac{1}{2L_A}\left(\frac{\hbar}{2e}\right)^2\phi_T^2 - \frac{\hbar}{2e}I\phi_T - \frac{\hbar^2}{2C_J}\left(\frac{2e}{\hbar}\right)^2\frac{\partial^2}{\partial\phi_J^2} + E_c(1-\cos\phi_J) + \frac{1}{2L_A}\left(\frac{\hbar}{2e}\right)^2\phi_J^2 - \frac{1}{L_A}\left(\frac{\hbar}{2e}\right)^2\phi_T\phi_J. \tag{8}$$

It is more convenient to work with dimensionless quantities. If $(L_AC_A)^{-1/2}$ is the resonant frequency of the antenna, which should be the same as the frequency of the absorbed photon, we may rescale the total Hamiltonian by what we shall call *the photon's energy* $\hbar/\sqrt{L_AC_A}$ and introduce the dimensionless Hamiltonian

$$\hat{H}_d^{(1)} = \frac{\sqrt{L_AC_A}}{\hbar}\hat{H}^{(1)} = -\frac{1}{2}\frac{(2e)^2}{\hbar}\sqrt{\frac{L_A}{C_A}}\frac{\partial^2}{\partial\phi_T^2} + \frac{1}{2}\frac{\hbar}{(2e)^2}\sqrt{\frac{C_A}{L_A}}\phi_T^2 - \frac{\sqrt{L_AC_A}}{2e}I\phi_T - \frac{1}{2}\frac{(2e)^2}{\hbar}\frac{\sqrt{L_AC_A}}{C_J}\frac{\partial^2}{\partial\phi_J^2}$$
$$+\frac{I_c\sqrt{L_AC_A}}{2e}(1-\cos\phi_J) + \frac{1}{2}\frac{\hbar}{(2e)^2}\sqrt{\frac{C_A}{L_A}}\phi_J^2 - \frac{\hbar}{(2e)^2}\sqrt{\frac{C_A}{L_A}}\phi_T\phi_J.$$

We denote

$$\tilde{\phi}_T \equiv \left(\frac{\hbar}{(2e)^2}\sqrt{\frac{C_A}{L_A}}\right)^{1/2}\phi_T, \quad \phi_J' \equiv \left(\frac{\hbar}{(2e)^2}\sqrt{\frac{C_J}{L_A}}\right)^{1/2}\phi_J$$

to write $\hat{H}_d^{(1)}$ in the simpler form

$$\hat{H}_d^{(1)} = -\frac{1}{2}\frac{\partial^2}{\partial\tilde{\phi}_T^2} + \frac{1}{2}\tilde{\phi}_T^2 - \left(\frac{L_A^3C_A}{\hbar^2}\right)^{1/4}I\tilde{\phi}_T + \sqrt{\frac{C_A}{C_J}}\left\{-\frac{1}{2}\frac{\partial^2}{\partial(\phi_J')^2} + \frac{I_c\sqrt{L_AC_J}}{2e}\left[1-\cos\left(\frac{\phi_J'}{\sqrt{\frac{\hbar}{(2e)^2}\sqrt{\frac{C_J}{L_A}}}}\right)\right] + \frac{1}{2}(\phi_J')^2\right\}$$
$$-\left(\frac{C_A}{C_J}\right)^{1/4}\tilde{\phi}_T\phi_J'. \tag{9}$$

Introducing the variable $\tilde{\phi}_J \equiv (C_J/C_A)^{1/4}\phi_J'$ and the notations $\omega_A \equiv (L_AC_A)^{-1/2}$, $Z_0 \equiv \frac{\hbar}{(2e)^2}$, and $Z_A \equiv \sqrt{L_A/C_A}$, we write the Hamiltonian (9) as

$$\hat{H}_d^{(1)} = -\frac{1}{2}\frac{\partial^2}{\partial\tilde{\phi}_T^2} - \frac{1}{2}\frac{\partial^2}{\partial\tilde{\phi}_J^2} + \frac{1}{2}\left(\tilde{\phi}_T - \sqrt{\frac{C_A}{C_J}}\tilde{\phi}_J\right)^2 - \left(\frac{L_A^3C_A}{\hbar^2}\right)^{1/4}I\tilde{\phi}_T + \frac{I_c\sqrt{L_AC_A}}{2e}\left[1-\cos\left(\frac{\tilde{\phi}_J}{\sqrt{\frac{\hbar}{(2e)^2}\frac{C_J}{\sqrt{L_AC_A}}}}\right)\right]$$
$$= -\frac{1}{2}\frac{\partial^2}{\partial\tilde{\phi}_T^2} - \frac{1}{2}\frac{\partial^2}{\partial\tilde{\phi}_J^2} + \frac{1}{2}\left(\tilde{\phi}_T - \sqrt{\frac{C_A}{C_J}}\tilde{\phi}_J - \frac{1}{2e\omega_A}\sqrt{\frac{Z_A}{Z_0}}I\right)^2 + \frac{I_c}{2e\omega_A}\left[1-\cos\left(\frac{\tilde{\phi}_J}{\sqrt{Z_0C_J\omega_A}}\right)\right] - \frac{1}{2e\omega_A}\frac{1}{\sqrt{Z_0C_J\omega_A}}I\tilde{\phi}_J$$
$$-\frac{1}{2}\frac{1}{(2e)^2\omega_A^2}\frac{Z_A}{Z_0}I^2. \tag{10}$$

We observe that the quantum particle moves in a 2D potential, which is parabolic along the direction $\tilde{\phi}_T - \sqrt{C_A/C_J}\tilde{\phi}_J$ and has a washboard shape along the direction $\tilde{\phi}_J$.

B. Second setup

We analyze now the second setup, similar to the one in Ref. [29]. A simplified version of the circuit is depicted in Fig. 2. In this case, the Hamiltonian for the JJ remains the same as Eq. (1a), with the modification that now the voltage on the JJ capacitor is the total voltage, i.e., $V_J \equiv V_T$. On the other hand, the energy of the antenna is

$$E_A = \frac{C_A V_A^2}{2} + \frac{L_A I_A^2}{2} \equiv \frac{Q_A^2}{2C_A} + \frac{L_A I_A^2}{2}. \tag{11}$$

The total energy of the system is given again by Eq. (1c). The total phase and the Hamiltonian are (2) and (3), respectively. If, like in Sec/II A, I_A is the current through the antenna, I_J is the current through the JJ, and I_{C_J} is the current through the capacitance of the JJ, then the current conservation reads

$$I = I_A + I_J + I_{C_J}. \tag{12}$$

Equation (12) couples the Hamiltonian of the antenna with the Hamiltonian of the JJ.

Denoting by V_{L_A} the voltage on the antenna inductance and by V_{C_A} the voltage on the antenna capacitance, we define the phases

$$\phi_{L_A} \equiv \frac{2e}{\hbar}\int_{-\infty}^{t} dt' V_{L_A}(t') = \frac{2e}{\hbar}\int_{-\infty}^{t} dt'\left[V_T(t') - \frac{Q_{C_A}(t')}{C_A}\right], \tag{13a}$$

$$\phi_{C_A} \equiv \frac{2e}{\hbar}\int_{-\infty}^{t} dt' V_{C_A}(t') = \frac{2e}{\hbar}\int_{-\infty}^{t} dt' \frac{Q_{C_A}(t')}{C_A}, \tag{13b}$$

$$\phi_J = \frac{2e}{\hbar}\int_{-\infty}^{t} dt' V_J(t') \equiv \frac{2e}{\hbar}\int_{-\infty}^{t} dt' V_T(t') \equiv \phi_T, \tag{13c}$$

which have to be embedded into the total Hamiltonian of the system,

$$E_T^{(2)} = \frac{Q_T^2}{2C_J} + E_c(1-\cos\phi_J) + \frac{Q_{C_A}^2}{2C_A} + \left(\frac{\hbar}{2e}\right)^2 \frac{\phi_{L_A}^2}{2L_A} - \frac{\hbar}{2e} I\phi_T, \tag{14}$$

where Q_T is the charge on the JJ capacitance. Using the relation $\phi_{L_A} \equiv \phi_T - \phi_{C_A}$, from (14) we obtain

$$E_T^{(2)} = \frac{Q_T^2}{2C_J} + E_c(1-\cos\phi_T) + \left(\frac{\hbar}{2e}\right)^2 \frac{\phi_T^2}{2L_A} - \frac{\hbar}{2e} I\phi_T + \frac{Q_{C_A}^2}{2C_A} + \left(\frac{\hbar}{2e}\right)^2 \frac{\phi_{C_A}^2}{2L_A} - \left(\frac{\hbar}{2e}\right)^2 \frac{\phi_T \phi_{C_A}}{L_A}. \tag{15}$$

From Eq. (15) we obtain the Hamiltonian

$$\hat{H}^{(2)} = -\frac{(2e)^2}{2C_J}\frac{\partial^2}{\partial\phi_T^2} + E_c(1-\cos\phi_T) + \left(\frac{\hbar}{2e}\right)^2 \frac{\phi_T^2}{2L_A} - \frac{\hbar}{2e} I\phi_T - \frac{(2e)^2}{2C_A}\frac{\partial^2}{\partial\phi_{C_A}^2} + \left(\frac{\hbar}{2e}\right)^2 \frac{\phi_{C_A}^2}{2L_A} - \left(\frac{\hbar}{2e}\right)^2 \frac{\phi_T \phi_{C_A}}{L_A}. \tag{16}$$

To make the Hamiltonian dimensionless, we divide Eq. (16) by the photon's energy and define

$$\hat{H}_d^{(2)} \equiv \frac{\hat{H}^{(2)}}{\hbar\omega_A} = -\frac{1}{2}\frac{1}{Z_0 C_J \omega_A}\frac{\partial^2}{\partial\phi_T^2} + \frac{I_c}{2e\omega_A}(1-\cos\phi_T) + \frac{1}{2}\frac{Z_0}{Z_A}\phi_T^2 - \frac{1}{2e\omega_A} I\phi_T - \frac{1}{2}\frac{Z_A}{Z_0}\frac{\partial^2}{\partial\phi_{C_A}^2} + \frac{1}{2}\frac{Z_0}{Z_A}\phi_{C_A}^2 - \frac{Z_0}{Z_A}\phi_T\phi_{C_A}. \tag{17}$$

Introducing the variables $\tilde{\phi}_T = \sqrt{Z_0 C_J \omega_A}\phi_T$ and $\tilde{\phi}_{C_A} = \sqrt{\frac{Z_0}{Z_A}}\phi_{C_A}$, we obtain

$$\hat{H}_d^{(2)} = -\frac{1}{2}\frac{\partial^2}{\partial\tilde{\phi}_T^2} - \frac{1}{2}\frac{\partial^2}{\partial\tilde{\phi}_{C_A}^2} + \frac{1}{2}\left(\tilde{\phi}_{C_A} - \sqrt{\frac{C_A}{C_J}}\tilde{\phi}_T\right)^2 + \frac{I_c}{2e\omega_A}\left[1-\cos\left(\frac{\tilde{\phi}_T}{\sqrt{Z_0 C_J \omega_A}}\right)\right] - \frac{1}{2e\omega_A}\frac{1}{\sqrt{Z_0 C_J \omega_A}} I\tilde{\phi}_T. \tag{18}$$

We observe that (making the identification $\tilde{\phi}_{C_A} \equiv \tilde{\phi}_J$) the Hamiltonian (18) is equivalent to the Hamiltonian (10), except that in (10) the potential energy is shifted by the constant value $-(L_A^3 C_A/2\hbar^2)^{1/2} I^2$ and is translated in the direction $\tilde{\phi}_J - \sqrt{C_A/C_J}\tilde{\phi}_T$ by $-\sqrt{Z_A/Z_0}I/(2e\omega_A)$. These differences are irrelevant for the dynamics of the quantum particle, and we shall see that all the physical results of the two setups are identical.

III. RESULTS

Having derived the Hamiltonians for the two configurations, we can calculate the local minima, the saddle points, and the energy required to excite the system over the saddle point.

A. Local minima and saddle points for the first setup

The particle described by the Hamiltonian $\hat{H}_d^{(1)}$ (10) of the first setup has a potential energy

$$U_d^{(1)} \equiv \frac{1}{2}\left[\tilde{\phi}_T - \sqrt{\frac{C_A}{C_J}}\tilde{\phi}_J - \frac{1}{2e\omega_A}\sqrt{\frac{Z_A}{Z_0}} I\right]^2 - \frac{1}{2}\frac{1}{(2e)^2\omega_A^2}\frac{Z_A}{Z_0} I^2 + \frac{I_c}{2e\omega_A}\left[1-\cos\left(\frac{\tilde{\phi}_J}{\sqrt{Z_0 C_J \omega_A}}\right)\right] - \frac{1}{2e\omega_A}\frac{1}{\sqrt{Z_0 C_J \omega_A}} I\tilde{\phi}_J. \tag{19}$$

As noticed before, along the $\tilde{\phi}_J$ direction we have a washboard potential, whereas along the $\tilde{\phi}_T - \sqrt{C_A/C_J}\tilde{\phi}_J$ direction we have a harmonic potential. The minima and the saddle points of these potentials are found by calculating the derivatives

$$\frac{\partial U_d^{(1)}}{\partial\tilde{\phi}_T} = \left(\tilde{\phi}_T - \sqrt{\frac{C_A}{C_J}}\tilde{\phi}_J\right) - \frac{1}{2e\omega_A}\sqrt{\frac{Z_A}{Z_0}} I, \tag{20a}$$

$$\frac{\partial^2 U_d^{(1)}}{\partial(\tilde{\phi}_T)^2} = 1, \tag{20b}$$

$$\frac{\partial^2 U_d^{(1)}}{\partial\tilde{\phi}_T\partial\tilde{\phi}_J} = -\sqrt{\frac{C_A}{C_J}}, \tag{20c}$$

$$\frac{\partial U_d^{(1)}}{\partial\tilde{\phi}_J} = -\sqrt{\frac{C_A}{C_J}}\left(\tilde{\phi}_T - \sqrt{\frac{C_A}{C_J}}\tilde{\phi}_J\right) + I_c\frac{1}{2e\omega_A}\frac{1}{\sqrt{Z_0C_J\omega_A}}\sin\left(\frac{\tilde{\phi}_J}{\sqrt{Z_0C_J\omega_A}}\right), \tag{20d}$$

$$\frac{\partial^2 U_d^{(1)}}{\partial\tilde{\phi}_J^2} = \frac{C_A}{C_J} + \frac{I_c}{2eZ_0C_J\omega_A^2}\cos\left(\frac{\tilde{\phi}_J}{\sqrt{Z_0C_J\omega_A}}\right). \tag{20e}$$

From Eqs. (20a) and (20d) we obtain the relations which have to be satisfied in the local minima and in the saddle points,

$$\frac{1}{2e\omega_A}\sqrt{\frac{Z_A}{Z_0}}I = \left(\tilde{\phi}_T - \sqrt{\frac{C_A}{C_J}}\tilde{\phi}_J\right), \tag{21a}$$

$$\frac{I}{I_c} = \sin\left(\frac{\tilde{\phi}_J}{\sqrt{Z_0C_J\omega_A}}\right). \tag{21b}$$

As expected, we observe that Eq. (21b) has a solution if and only if $-1 < I/I_c < 1$. If we choose only positive currents ($I \geqslant 0$), then the local minima are at

$$\tilde{\phi}_{J,\min} = \sqrt{Z_0C_J\omega_A}\left[\arcsin\left(\frac{I}{I_c}\right) + 2n\pi\right], \tag{22a}$$

$$\tilde{\phi}_{T,\min} = \frac{1}{2e\omega_A}\sqrt{\frac{Z_A}{Z_0}}I + \sqrt{\frac{Z_0}{Z_A}}\left[\arcsin\left(\frac{I}{I_c}\right) + 2n\pi\right] \tag{22b}$$

(where n is an integer), whereas the saddle points are at

$$\tilde{\phi}_{J,\text{saddle}} = \sqrt{Z_0C_J\omega_A}\left[(2n+1)\pi - \arcsin\left(\frac{I}{I_c}\right)\right], \tag{23a}$$

$$\tilde{\phi}_{T,\text{saddle}} = \frac{I}{2e\omega_A}\sqrt{\frac{Z_A}{Z_0}} + \sqrt{\frac{Z_0}{Z_A}}\left[(2n+1)\pi - \arcsin\left(\frac{I}{I_c}\right)\right]. \tag{23b}$$

The second derivatives in the minima are

$$\frac{\partial^2 U_d^{(1)}}{\partial(\tilde{\phi}_T)^2} = 1, \tag{24a}$$

$$\frac{\partial^2 U_d^{(1)}}{\partial\tilde{\phi}_T\partial\tilde{\phi}_J} = -\sqrt{\frac{C_A}{C_J}} = \frac{\partial^2 U_d^{(1)}}{\partial\tilde{\phi}_J\partial\tilde{\phi}_T}, \tag{24b}$$

$$\frac{\partial^2 U_d^{(1)}}{\partial\tilde{\phi}_J^2} = \frac{C_A}{C_J} + \frac{I_c}{2eZ_0C_J\omega_A^2}\sqrt{1-\frac{I^2}{I_c^2}}. \tag{24c}$$

The values of the potential energy at the minima and the saddle points are

$$U_{d,\min}^{(1)}(n) = -\frac{1}{2}\frac{1}{(2e)^2\omega_A^2}\frac{Z_A}{Z_0}I^2 + \frac{I_c}{2e\omega_A}\left[1-\sqrt{1-\frac{I^2}{I_c^2}}\right] - \frac{I}{2e\omega_A}\left[\arcsin\left(\frac{I}{I_c}\right) + 2n\pi\right], \tag{25a}$$

$$U_{d,\text{saddle}}^{(1)}(n) = -\frac{1}{2}\frac{1}{(2e)^2\omega_A^2}\frac{Z_A}{Z_0}I^2 + \frac{I_c}{2e\omega_A}\left[1+\sqrt{1-\frac{I^2}{I_c^2}}\right] - \frac{I}{2e\omega_A}\left[(2n+1)\pi - \arcsin\left(\frac{I}{I_c}\right)\right], \tag{25b}$$

respectively. The energy difference between a saddle point and the closest local minimum is

$$U_{d,\text{saddle}}^{(1)}(n) - U_{d,\min}^{(1)}(n) = \frac{I_c}{e\omega_A}\left\{\sqrt{1-\frac{I^2}{I_c^2}} - \frac{I}{I_c}\left[\frac{\pi}{2} - \arcsin\left(\frac{I}{I_c}\right)\right]\right\}. \tag{26}$$

B. Local minima and saddle points for the second setup

For the second configuration, from Eq. (18) we obtain the potential energy

$$U_d^{(2)} = \frac{1}{2}\left(\tilde{\phi}_{C_A} - \sqrt{\frac{C_A}{C_J}}\tilde{\phi}_T\right)^2 + \frac{I_c}{2e\omega_A}\left[1-\cos\left(\frac{\tilde{\phi}_T}{\sqrt{Z_0C_J\omega_A}}\right)\right] - \frac{I}{2e\omega_A}\frac{1}{\sqrt{Z_0C_J\omega_A}}\tilde{\phi}_T. \tag{27}$$

Since $U_d^{(2)}$ has the same shape as $U_d^{(1)}$, but with different variables, the analysis is similar to the one in Sec. III A. For this reason, we state here only the main results. Along the $\tilde{\phi}_T$ direction we have a washboard potential, which has local minima if and only if $-1 < I/I_c < 1$. We work again with $I \geqslant 0$, and we have the coordinates

$$\tilde{\phi}_{T,\min} = \sqrt{Z_0C_J\omega_A}\left[\arcsin\left(\frac{I}{I_c}\right) + 2n\pi\right], \tag{28a}$$

$$\tilde{\phi}_{C_A,\min} = \sqrt{\frac{Z_0}{Z_A}}\left[\arcsin\left(\frac{I}{I_c}\right) + 2n\pi\right] \tag{28b}$$

for local minima and

$$\tilde{\phi}_{T,\text{saddle}} = \sqrt{Z_0C_J\omega_A}\left[(2n+1)\pi - \arcsin\left(\frac{I}{I_c}\right)\right], \tag{29a}$$

$$\tilde{\phi}_{C_A,\text{saddle}} = \sqrt{\frac{Z_0}{Z_A}}\left[(2n+1)\pi - \arcsin\left(\frac{I}{I_c}\right)\right] \tag{29b}$$

for saddle points. The second derivatives in the minimum energy points are identical to the ones calculated in Sec. III A (but with different coordinates), namely,

$$\frac{\partial^2 U_d^{(2)}}{\partial\tilde{\phi}_{C_A}^2} = 1, \tag{30a}$$

$$\frac{\partial^2 U_d^{(2)}}{\partial\tilde{\phi}_{C_A}\partial\tilde{\phi}_T} = -\sqrt{\frac{C_A}{C_J}} = \frac{\partial^2 U_d^{(2)}}{\partial\tilde{\phi}_T\partial\tilde{\phi}_{C_A}}, \tag{30b}$$

$$\frac{\partial^2 U_d^{(2)}}{\partial\tilde{\phi}_T^2} = \frac{C_A}{C_J} + \frac{I_c}{2eZ_0C_J\omega_A^2}\sqrt{1-\frac{I^2}{I_c^2}}. \tag{30c}$$

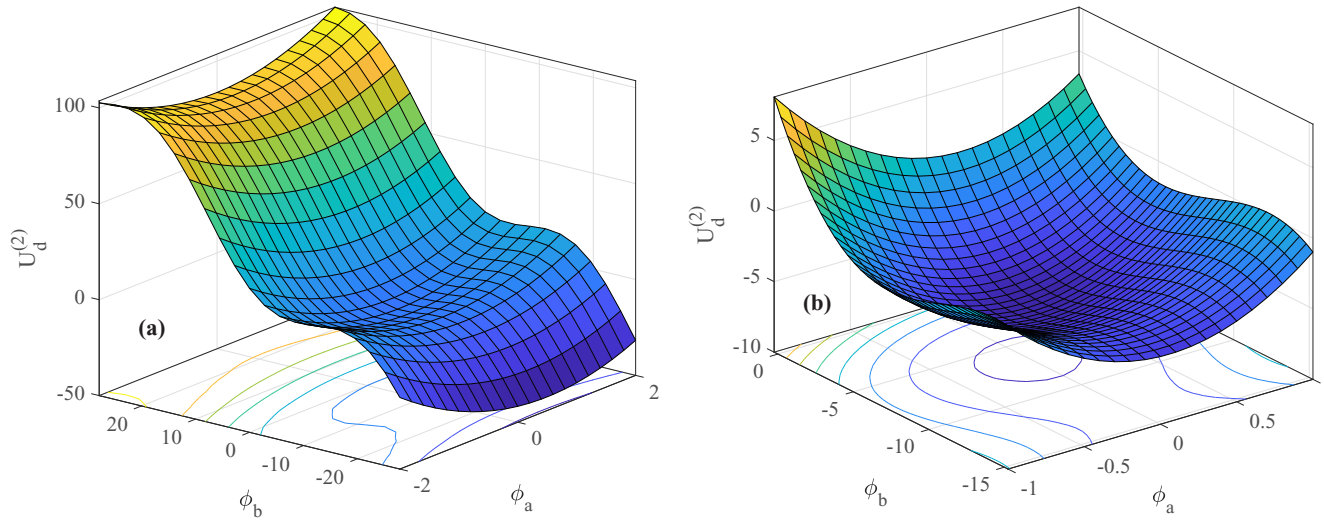

FIG. 3. The potential energy $U_d^{(2)}$ in the rotated system of coordinates (ϕ_1, ϕ_2). The parameters take typical values $I_c = 1\,\mu$A, $C_A = C_J = 1$ pF [25,26], and $\omega_A/(2\pi) = 30$ GHz. The value $I/I_c \approx 0.85$ will be justified later. One can observe that the potential is very asymmetric in the variables ϕ_1 and ϕ_2. The plot in (b) is a detail of the plot in (a), emphasizing a local minimum.

The values of the energy at the minima and at the saddle points are

$$U^{(2)}_{d,\min}(n) = \frac{I_c}{2e\omega_A}\left[1-\sqrt{1-\frac{I^2}{I_c^2}}\right] - \frac{I}{2e\omega_A}\left[\arcsin\left(\frac{I}{I_c}\right)+2n\pi\right], \tag{31a}$$

$$U^{(2)}_{d,\text{saddle}}(n) = \frac{I_c}{2e\omega_A}\left[1+\sqrt{1-\frac{I^2}{I_c^2}}\right] - \frac{I}{2e\omega_A}\left[(2n+1)\pi-\arcsin\left(\frac{I}{I_c}\right)\right], \tag{31b}$$

respectively. As expected, $U^{(2)}_{d,\min}(n) - U^{(1)}_{d,\min}(n) = U^{(2)}_{d,\text{saddle}}(n) - U^{(1)}_{d,\text{saddle}}(n) = (Z_A/Z_0)I^2/[2(2e\omega_A)^2]$, which implies that $U^{(2)}_{d,\text{saddle}}(n) - U^{(2)}_{d,\min}(n) = U^{(1)}_{d,\text{saddle}}(n) - U^{(1)}_{d,\min}(n)$ [see Eq. (26)].

IV. DISCUSSION

Although the Hamiltonians (8) and (16), which describe the two schematic setups in Figs. 1 and 2, respectively, are apparently different, we saw in Sec. III that, by dividing them by $\hbar/\sqrt{L_A C_A}$ and changing the variables, they can be reduced to dimensionless Hamiltonians that represent quantum particles of unit mass in potential landscapes which are translated with respect to each other. A small part of $U_d^{(2)}$ is presented in Fig. 3. The system of coordinates is rotated to (ϕ_a, ϕ_b), defined as

$$\phi_a \equiv \frac{\tilde\phi_{C_A} - \sqrt{C_A/C_J}\tilde\phi_T}{\sqrt{1+C_A/C_J}}, \quad \phi_b \equiv \frac{\sqrt{C_A/C_J}\tilde\phi_{C_A} + \tilde\phi_T}{\sqrt{1+C_A/C_J}}, \tag{32}$$

because in the original coordinates the local potential well is too narrow to be clearly seen.

In the initial state (before the absorption of the photon), the quantum particle may sit in the metastable ground state of the local minimum represented in Fig. 3(b). The energy difference between the local minimum and the nearest saddle point is the same in both setups and can be obtained from Eq. (26), which gives

$$\epsilon^{(1)}_{\text{ph}} \equiv \hbar\omega_A\big(U^{(2)}_{d,\text{saddle}} - U^{(2)}_{d,\min}\big) = \hbar\omega_A\big(U^{(1)}_{d,\text{saddle}} - U^{(1)}_{d,\min}\big) = 4eI_cZ_0\left\{\sqrt{1-\frac{I^2}{I_c^2}} - \frac{I}{I_c}\left[\frac{\pi}{2}-\arcsin\left(\frac{I}{I_c}\right)\right]\right\}. \tag{33}$$

To calculate the energy of the photon required to excite the system from the metastable ground state of a local minimum over the saddle point, we approximate the potential energy in the local minimum with a harmonic potential. The second derivatives of the potential energies $U_d^{(1)}$ and $U_d^{(2)}$ in the local minima are identical, Eqs. (24) and (30), so we can analyze only one of them. If a local minimum is located at $(\tilde\phi_{J,\min}, \tilde\phi_{T,\min})$, we denote $\phi_1 \equiv \tilde\phi_J - \tilde\phi_{J,\min}$ and $\phi_2 \equiv \tilde\phi_T - \tilde\phi_{T,\min}$. In the new variables and in the harmonic approximation around $(\tilde\phi_{J,\min}, \tilde\phi_{T,\min})$, both Hamiltonians $H_d^{(1)}$ and $H_d^{(2)}$ become (neglecting constant terms)

$$\hat H_d \equiv -\frac{1}{2}\frac{\partial^2}{\partial\phi_1^2} - \frac{1}{2}\frac{\partial^2}{\partial\phi_2^2} + \frac{1}{2}\left(\frac{C_A}{C_J} + \frac{I_c}{2eZ_0C_J\omega_A^2}\sqrt{1-\frac{I^2}{I_c^2}}\right)\phi_1^2 - \sqrt{\frac{C_A}{C_J}}\phi_1\phi_2 + \frac{1}{2}\phi_2^2. \tag{34}$$

Denoting

$$a \equiv \frac{C_A}{C_J} + \frac{I_c}{2eZ_0C_J\omega_A^2}\sqrt{1-\frac{I^2}{I_c^2}}, \tag{35a}$$

$$D \equiv \sqrt{(a-1)^2 + 4\frac{C_A}{C_J}}, \tag{35b}$$

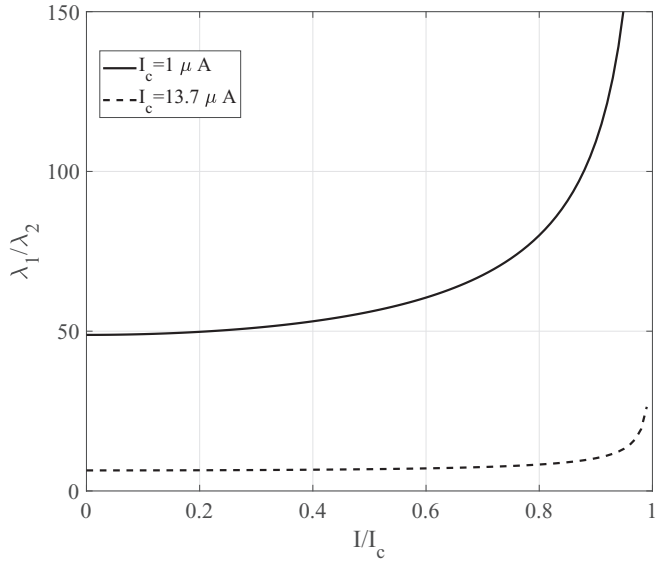

FIG. 4. The ratio λ_1/λ_2 for $I_c = 1\,\mu$A (solid line), $I_c = 13.7\,\mu$A (dashed line), $C_A = C_J = 1$ pF, and $\omega_A/(2\pi) = 30$ GHz (notice that $\lambda_2 \to 0$ when $I/I_c \nearrow 1$).

we define the orthogonal vectors

$$v_1 \equiv \frac{\phi_1 + \sqrt{\frac{C_J}{C_A}}\frac{1-a+D}{2}\phi_2}{\sqrt{1+\frac{C_J}{C_A}\frac{(1-a+D)^2}{4}}}, \quad v_2 \equiv \frac{\phi_1 + \sqrt{\frac{C_J}{C_A}}\frac{1-a-D}{2}\phi_2}{\sqrt{1+\frac{C_J}{C_A}\frac{(1-a-D)^2}{4}}}, \tag{36}$$

which diagonalize the Hamiltonian (34), bringing it to the form

$$\hat{H}_d = -\frac{1}{2}\frac{\partial^2}{\partial v_1^2} - \frac{1}{2}\frac{\partial^2}{\partial v_2^2} + \frac{1}{2}\lambda_1 v_1^2 + \frac{1}{2}\lambda_2 v_2^2, \tag{37a}$$

where

$$\lambda_1 \equiv \tfrac{1}{2}(1+a+D), \quad \lambda_2 \equiv \tfrac{1}{2}(1+a-D). \tag{37b}$$

The Hamiltonian $\hat{H}_d$ of Eq. (37a) may be split into two Hamiltonians, $\hat{H}_d \equiv \hat{H}_{dA} + \hat{H}_{dB}$, where

$$\hat{H}_{dA} \equiv -\frac{1}{2}\frac{\partial^2}{\partial v_1^2} + \frac{1}{2}\lambda_1 v_1^2, \quad \hat{H}_{dB} \equiv -\frac{1}{2}\frac{\partial^2}{\partial v_2^2} + \frac{1}{2}\lambda_2 v_2^2. \tag{37c}$$

We observe that at $I/I_c = 1$, $\lambda_1 = 2$, and $\lambda_2 = 0$ for any values of the parameters. For $I/I_c \in [0, 1)$, the ratio λ_1/λ_2 is plotted in Fig. 4 for two values of I_c.

Using Eqs. (37) and taking into account the rescaling of the Hamiltonians $H^{(1)}$ and $H^{(2)}$ by $\hbar\omega_A$, we obtain their common eigenvalues in the harmonic approximation,

$$\epsilon_{\rm QMT}(m,n) = \hbar\omega_A\left[\sqrt{\lambda_1}\left(m+\tfrac{1}{2}\right) + \sqrt{\lambda_2}\left(n+\tfrac{1}{2}\right)\right]. \tag{38}$$

When $\lambda_1 \gg \lambda_2$ (see Fig. 4), mostly the first term will contribute to the ground-state energy of the particle, whereas the second term may play a role in the thermal excitation if the device works at temperatures comparable to $\sqrt{\lambda_2}\hbar\omega_A/k_B$ but much smaller than $\sqrt{\lambda_1}\hbar\omega_A/k_B$.

If the system is prepared in the ground state in one of the local minima of the potential, then the excitation energy required to get into the running state over the potential barrier (see Fig. 3) is calculated from Eqs. (33) and (38) to be

$$\epsilon_{\rm ph} = \epsilon_{\rm ph}^{(1)} - \epsilon_{\rm QMT}(0,0) \equiv \Delta U. \tag{39}$$

For typical values of the parameters $I_c = 1\,\mu$A and $C_A = C_J = 1$ pF [25,26], choosing $\omega_A/(2\pi) = 30$ GHz, from Eq. (39) we obtain $I/I_c \approx 0.8523$ (so the bias current is quite close to the critical current). To be able to detect photons of energy $\hbar\omega_A$, the temperature T of the system and of the environment should be significantly lower than $T_A \equiv \hbar\omega_A/k_B \approx 1.4398$ K. The angular frequencies of the two independent oscillators of Eq. (38) are $\omega_1 \equiv \lambda_1\omega_A$ and $\omega_2 \equiv \lambda_2\omega_A$. For the chosen parameters, $\lambda_1 = 2.0226$ and $\lambda_2 = 0.0221$, so if $T \ll \hbar\omega_A/k_B$, oscillator 1 should be in the ground state at temperature T. Nevertheless, since $\lambda_2 \ll \lambda_1$, oscillator 2 could be in an excited state if T is comparable to or higher than $T_2 = \lambda_2\hbar\omega_2/k_B$. To check the harmonic approximation, we compare $\epsilon_{\rm ph}$ with $\epsilon_{\rm ph}^{(1)}$, and we obtain $\epsilon_{\rm QMT}(0,0)/(\hbar\omega_A) \approx 1.0080$. This implies $\epsilon_{\rm QMT}(0,0)/\epsilon_{\rm ph}^{(1)} \approx \epsilon_{\rm ph}/\epsilon_{\rm ph}^{(1)} \approx 0.5$, so the harmonic approximation is reasonably well justified.

The choices of parameters of the JJ which meet the criterion (39) are broad. For example, if the critical current is $I_c = 13.7\,\mu$A [25,26], then from Eq. (39) we obtain $I/I_c = 0.9729$, so the relative value of the bias current is much closer to 1 than in the previous case. In this case, $\lambda_1 \approx 2.3523$, and $\lambda_2 \approx 0.2605$, so as can be seen in Fig. 4, the ratio λ_1/λ_2 is not as big as for $I_c = 1\,\mu$A. Furthermore, $\epsilon_{\rm QMT}(0,0)/(\hbar\omega_A) \approx 1.1094$, and $\epsilon_{\rm QMT}(0,0)/\epsilon_{\rm ph}^{(1)} \approx 0.5259$, so the harmonic approximation is, again, quite well justified.

Dark counts

In the absence of the additional energy coming from the photon or from the thermal bath, the easiest escape route for the phase particle from the potential well is to tunnel through the saddle point region. To estimate the escape rate, we write the Hamiltonian $H^{(2)}$ using the variables ϕ_a and ϕ_b (32) and emphasize the washboard potential. In these variables, Eq. (18) becomes

$$\begin{aligned}\hat{H}_d^{(2)}(\phi_a,\phi_b) = &-\frac{1}{2}\frac{\partial^2}{\partial\phi_a^2} - \frac{1}{2}\frac{\partial^2}{\partial\phi_b^2} + \frac{1}{2}\left(1+\frac{C_A}{C_J}\right)\phi_a^2 \\ &+\frac{I_c}{2e\omega_A}\left[1-\cos\left(\frac{-\sqrt{C_A/C_J}\phi_a+\phi_b}{\sqrt{Z_0C_J\omega_A(1+C_A/C_J)}}\right)\right] \\ &-\frac{I}{2e\omega_A}\frac{-\sqrt{C_A/C_J}\phi_a+\phi_b}{\sqrt{Z_0C_J\omega_A(1+C_A/C_J)}}.\end{aligned} \tag{40}$$

From Eqs. (28) and (29) we see that the local minima and the saddle points are located along the ϕ_b axis ($\phi_a = 0$). Along this axis ($\phi_a = 0$)—multiplying the Hamiltonian by $\hbar\omega_A$ to go back to $H^{(2)}$ in energy units and defining $\tilde{\phi}_b \equiv 2e/\sqrt{2C_J\hbar\omega_A(1+C_A/C_J)}$—we obtain

$$\begin{aligned}\hat{H}^{(2)}(0,\phi_b) = &-\frac{(2e)^2}{2C_J(1+C_A/C_J)}\frac{\partial^2}{\partial\tilde{\phi}_b^2} \\ &-E_c\left[\frac{I}{I_c}\tilde{\phi}_b + \cos\left(\tilde{\phi}_b\right)\right] + E_c,\end{aligned} \tag{41}$$

which describes a (phase) particle in a washboard potential. We notice that the "mass" of this particle became bigger than the mass of the Josephson particle by $1 + C_A/C_J$ (≈ 2 for our choice of parameters) due to the presence of the antenna. In such a situation, we shall estimate the order of magnitude of the escape rates as usual in the model of Caldeira and Leggett [38], considering the tunneling along this axis. A more detailed analysis of the escape rate in a 2D potential will be done elsewhere.

The escape rate, taking into account the dissipation, may be calculated as [25,38]

$$\Gamma = \frac{\omega_0}{2\pi}\sqrt{\frac{B}{2\pi}}e^{-B}, \tag{42}$$

where $B = \Delta U/(\hbar\omega_0)(7.2 + 8A/Q)$, $Q = \omega_0 RC$ is the quality factor, A is a numerical parameter, R is the shunt resistance of the junction, and $\Delta U = \hbar\omega_A$ is the height of the potential barrier at the saddle point given by Eq. (39); the angular frequency $\omega_0 = \omega_A\sqrt{\lambda_2}$ corresponds to the local minimum of the one-dimensional potential (41). Using the numerical values from [25] for an estimation ($R = 0.44\,\mathrm{k}\Omega$ and $A = 10$), we obtain

$$\Gamma_1 \approx 1.8 \times 10^{-30}\,\mathrm{Hz} \tag{43}$$

for the first case ($I_c = 1\,\mu\mathrm{A}$) and

$$\Gamma_2 \approx 1.7 \times 10^{-2}\,\mathrm{Hz} \tag{44}$$

for the second case ($I_c = 13.7\,\mu\mathrm{A}$). We observe that only in the first case is the escape rate low enough to allow a counting rate of one photon in a few hours. Therefore, the escape rate imposes an additional constraint for the choice of the JJ parameters, besides Eq. (39).

V. CONCLUSIONS

We studied theoretically the possibility of counting microwave photons with a detector consisting of a Josephson junction coupled to an antenna. In this paper, we focused on the derivation of the effective Hamiltonian of the device. Its quantum dynamics, including the interplay between activation and tunneling, as well as thermalization after an absorption event, will be considered elsewhere. Such an analysis will allow the estimation of the dead time of the detector after the counting of a photon.

We analyzed two configurations. In the first one, the JJ is connected in series with the antenna and is similar to the photon counter with a cold-electron bolometer [24,32], in which the CEB is replaced by the JJ. In the second configuration, the JJ is capacitively coupled to the antenna and is similar to the one used in [29], for example. For the two configurations, we constructed simple equivalent electric circuits, and we wrote the Hamiltonians in the macroscopic quantum tunneling formalism. In this formalism, the dynamics of the JJ is described as a quantum particle moving in a two-dimensional potential landscape. After appropriate changes of coordinates, the Schrödinger equations describing the two setups were put into equivalent forms, which implies that they have the same quantum-mechanical properties.

The potential landscape in which the quantum particle is moving has the shape of a washboard potential in one direction and is parabolic in another direction; these two directions are not perpendicular to each other [see Eqs. (19) and (27)]. If the bias current is smaller than the critical current of the junction, the washboard potential forms (as in the one-dimensional case) an infinite chain of local minima, in which the quantum particle can be placed in an initial metastable state (see Fig. 3). The local minima are separated by potential barriers, and the minimum of each potential barrier is a saddle point.

To calculate analytically the metastable states (especially the "ground state"), in the vicinity of a local minimum we approximate the potential energy by a harmonic potential. At low temperatures, the particle is assumed to be initially in the ground state of a local minimum. When the photon is absorbed, the particle is excited. If the excitation energy is larger than the difference between the energy of the saddle point and the ground-state energy in the closest local minimum, then the system may get into the running state, and the photon is detected.

We calculated the parameters of the device which would allow it to detect 1-cm-wavelength photons. If the critical current of the junction is $I_c = 1\,\mu\mathrm{A}$ and $C_A = C_J = 1$ pF, then the bias current I should satisfy the condition $0.8523 I_c \leqslant I < I_c$ to ensure that the photon is able to excite the particle over the potential barrier. As another example, we took $I_c = 13.7\,\mu\mathrm{A}$, and in this case (keeping $C_A = C_J = 1$ pF) we obtained $0.9729 I_c \leqslant I < I_c$ to be able to detect the 1-cm-wavelength photon.

The photon energy ϵ_{ph} does not have to be larger than the potential energy barrier ΔU to be detected. By exciting the JJ to a state of higher energy, even if that energy is lower than the potential barrier, the phase particle may get into the running state by tunneling into the continuum. The tunneling rate increases rapidly with the energy of the phase particle.

The tunneling process may also cause *dark counts* when the phase particle tunnels the potential barrier directly from the ground state, that is, in the absence of a photon. This was estimated in Sec. IV, and it turned out that only in the first case ($I_c = 1\,\mu\mathrm{A}$) is the dark count rate low enough to permit the observation of one relevant photon (produced by the axion's decay) in a few hours, whereas in the second case ($I_c = 13.7\,\mu\mathrm{A}$) the dark count rate is of the order of 1/min, so the detector may not be used for axion detection. Therefore, even if the parameters of the junction and the bias current may be tuned so that the photon excites the phase particle above the saddle point energy, the dark count rates impose stringent conditions in setting up the working point of the JJ axion (microwave photon) counter. Nevertheless, in experiments in which the flux of incoming microwave photons is higher (so that the dark count rate does not have to be so low), the JJ single-photon counter offers much more flexibility.

ACKNOWLEDGMENTS

This work was supported by the Executive Agency for Higher Education, Research, Development and Innovation Funding (UEFISCDI) (Project No. PN-19060101/2019)) and Romania-Joint Institute for Nuclear Research (JINR) collaboration projects, positions 23, 24, 26, Order No. 397/27.05.2019 (IFIN-HH) and the Russian Science Foundation (Project No. 16-19-10468).

[1] F. Giazotto, T. T. Heikkilä, A. Luukanen, A. M. Savin, and J. P. Pekola, Opportunities for mesoscopics in thermometry and refrigeration: Physics and applications, Rev. Mod. Phys. **78**, 217 (2006).

[2] R. H. Hadfield, Single-photon detectors for optical quantum information applications, Nat. Photonics **3**, 696 (2009).

[3] B. R. Johnson, M. D. Reed, A. A. Houck, D. I. Schuster, L. S. Bishop, E. Ginossar, J. M. Gambetta, L. DiCarlo, L. Frunzio, S. M. Girvin, and R. J. Schoelkopf, Quantum non-demolition detection of single microwave photons in a circuit, Nat. Phys. **6**, 663 (2010).

[4] E. A. Dauler, M. E. Grein, A. J. Kerman, F. Marsili, S. Miki, S. W. Nam, M. D. Shaw, H. Terai, V. B. Verma, and T. Yamashita, Review of superconducting nanowire single-photon detector system design options and demonstrated performance, Opt. Eng. **53**, 081907 (2014).

[5] M. D. Eisaman, J. Fan, A. Migdall, and S. V. Polyakov, Invited review article: Single-photon sources and detectors, Rev. Sci. Instrum. **82**, 071101 (2011).

[6] S. Kono, K. Koshino, Y. Tabuchi, A. Noguchi, and Y. Nakamura, Quantum non-demolition detection of an itinerant microwave photon, Nat. Phys. **14**, 546 (2018).

[7] J.-C. Besse, S. Gasparinetti, M. C. Collodo, Th. Walter, P. Kurpiers, M. Pechal, C. Eichler, and A. Wallraff, Single-Shot Quantum Nondemolition Detection of Individual Itinerant Microwave Photons, Phys. Rev. X **8**, 021003 (2018).

[8] B. Royer, A. L. Grimsmo, A. Choquette-Poitevin, and A. Blais, Itinerant Microwave Photon Detector, Phys. Rev. Lett. **120**, 203602 (2018).

[9] A. Opremcak, I. V. Pechenezhskiy, C. Howington, B. G. Christensen, M. A. Beck, E. Leonard, J. Suttle, C. Wilen, K. N. Nesterov, G. J. Ribeill, T. Thorbeck, F. Schlenker, M. G. Vavilov, B. L. T. Plourde, and R. McDermott, Measurement of a superconducting qubit with a microwave photon counter, Science **361**, 1239 (2018).

[10] R. D. Peccei and H. R. Quinn, CP Conservation in the Presence of Pseudoparticles, Phys. Rev. Lett. **38**, 1440 (1977).

[11] R. D. Peccei and H. R. Quinn, Constraints imposed by CP conservation in the presence of pseudoparticles, Phys. Rev. D **16**, 1791 (1977).

[12] S. Weinberg, A New Light Boson? Phys. Rev. Lett. **40**, 223 (1978).

[13] F. Wilczek, Problem of Strong P and T Invariance in the Presence of Instantons, Phys. Rev. Lett. **40**, 279 (1978).

[14] P. Sikivie, Experimental Tests of the "Invisible" Axion, Phys. Rev. Lett. **51**, 1415 (1983).

[15] R. Barbieri, C. Braggio, G. Carugno, C. S. Gallo, A. Lombardi, A. Ortolan, R. Pengo, G. Ruoso, and C. C. Speake, Searching for galactic axions through magnetized media: The QUAX proposal, Phys. Dark Univ. **15**, 135 (2017).

[16] S. Anders, M. G. Blamire, F.-Im. Buchholz, D.-G. Crété, R. Cristiano, P. Febvre, L. Fritzsch, A. Herr, E. Il'ichev, J. Kohlmann, J. Kunert, H.-G. Meyer, J. Niemeyer, T. Ortlepp, H. Rogalla, T. Schurig, M. Siegel, R. Stolz, E. Tarte, H. J. M. ter Brake, H. Toepfer, J.-C. Villegier, A. M. Zagoskin, and A. B. Zorin, European roadmap on superconductive electronics–Status and perspectives, Phys. C (Amsterdam, Neth.) **470**, 2079 (2010).

[17] Y.-F. Chen, D. Hover, S. Sendelbach, L. Maurer, S. T. Merkel, E. J. Pritchett, F. K. Wilhelm, and R. McDermott, Microwave Photon Counter Based on Josephson Junctions, Phys. Rev. Lett. **107**, 217401 (2011).

[18] G. Romero, J. J. García-Ripoll, and E. Solano, Microwave Photon Detector in Circuit QED, Phys. Rev. Lett. **102**, 173602 (2009).

[19] G. Romero, J. J. García-Ripoll, and E. Solano, Photodetection of propagating quantum microwaves in circuit QED, Phys. Scr. **T137**, 014004 (2009).

[20] H. Takayanagi, Photon-assisted macroscopic quantum tunneling in a small Josephson junction, Phys. B (Amsterdam, Neth.) **165–166**, 959 (1990).

[21] L. Kuzmin, Optimization of the hot-electron bolometer and a cascade quasiparticle amplifier for space astronomy, in *The International Workshop on Superconducting Nano-electronics Devices*, edited by J. Pekola, B. Ruggiero, and P. Silvestrini (Springer, Boston, 2002), p. 145.

[22] L. Kuzmin, An array of cold-electron bolometers with SIN tunnel junctions and JFET readout for cosmology instruments, J. Phys.: Conf. Ser. **97**, 012310 (2008).

[23] M. A. Tarasov, L. S. Kuzmin, V. S. Edelman, S. Mahashabde, and P. de Bernardis, Optical response of a cold-electron bolometer array integrated in a 345-GHz cross-slot antenna, IEEE Trans. Appl. Supercond. **21**, 3635 (2011).

[24] D. V. Anghel and L. Kuzmin, Capacitively coupled hot-electron nanobolometer as far-infrared photon counter, Appl. Phys. Lett. **82**, 293 (2003).

[25] G. Oelsner, L. S. Revin, E. Il'ichev, A. L. Pankratov, H.-G. Meyer, L. Grönberg, J. Hassel, and L. S. Kuzmin, Underdamped Josephson junction as a switching current detector, Appl. Phys. Lett. **103**, 142605 (2013).

[26] G. Oelsner, C. K. Andersen, M. Rehák, M. Schmelz, S. Anders, M. Grajcar, U. Hübner, K. Mølmer, and E. Il'ichev, Detection of Weak Microwave Fields with an Underdamped Josephson Junction, Phys. Rev. Appl. **7**, 014012 (2017).

[27] A. Wallraff, D. I. Schuster, A. Blais, L. Frunzio, R.-S. Huang, J. Majer, S. Kumar, S. M. Girvin, and R. J. Schoelkopf, Strong coupling of a single photon to a superconducting qubit using circuit quantum electrodynamics, Nature (London) **431**, 162 (2004).

[28] C. K. Andersen and K. Mølmer, Effective description of tunneling in a time-dependent potential with applications to voltage switching in Josephson junctions, Phys. Rev. A **87**, 052119 (2013).

[29] C. K. Andersen, G. Oelsner, E. Il'ichev, and K. Mølmer, Quantized resonator field coupled to a current-biased Josephson junction in circuit QED, Phys. Rev. A **89**, 033853 (2014).

[30] E. V. Il'ichev, A microwave photon detector, Phys. Solid State **58**, 2160 (2016).

[31] A. Poudel, R. McDermott, and M. G. Vavilov, Quantum efficiency of a microwave photon detector based on a current-biased Josephson junction, Phys. Rev. B **86**, 174506 (2012).

[32] D. V. Anghel and L. S. Kuzmin, Cold electron bolometer, as a 1 cm wavelength photon counter, arXiv:1811.05326 [Phys. Rev. Appl. (to be published)].

[33] M. Nahum, T. M. Eiles, and J. M. Martinis, Electronic microrefrigerator based on a normal-insulator-superconductor tunnel junction, Appl. Phys. Lett. **65**, 3123 (1994).

[34] M. M. Leivo, J. P. Pekola, and D. V. Averin, Efficient Peltier refrigeration by a pair of normal metal/insulator/superconductor junctions, Appl. Phys. Lett. **68**, 1996 (1996).

[35] B. D. Josephson, Possible new effects in superconductive tunneling, Phys. Lett. **1**, 251 (1962).

[36] K. Likharev, *Dynamics of Josephson Junctions and Circuits* (Gordon and Breach, New York, 1986).

[37] G.-L. Ingold and Yu. V. Nazarov, Charge tunneling rates in ultrasmall junctions, arXiv:cond-mat/0508728.

[38] A. O. Caldeira and A. J. Leggett, Influence of Dissipation on Quantum Tunneling in Macroscopic Systems, Phys. Rev. Lett. **46**, 211 (1981).